RSC Advances

PAPER

View Article Online
View Journal | View Issue

Cite this: *RSC Adv.*, 2024, **14**, 14665

Synthesis of cobalt phosphide hybrid for simultaneous electrochemical detection of ascorbic acid, dopamine, and uric acid†

Hongyan Xu, Yulu Hang, Xiaoyu Lei, Jinan Deng * and Jun Yang *

Ascorbic acid (AA), dopamine (DA), and uric acid (UA) are important biomarkers for the clinical screening of diseases. However, the simultaneous determination of these three analytes is still challenging. Herein, we report a facile metal–organic framework (MOF)-derived method to synthesize a cobalt phosphide (Co_2P) hybrid for the simultaneous electrochemical detection of AA, DA and UA. The introduction of highly dispersed Co_2P nanoparticles onto a P, N-doped porous carbon matrix is responsible for providing abundant active sites and facilitating electron transfer, thereby contributing to the improved electrocatalytic performance of the hybrid. Well-resolved oxidation peaks and an enhanced current response for the simultaneous oxidation of AA, DA, and UA were achieved using a Co_2P hybrid-modified screen-printed electrode (Co_2P hybrid-SPE) with the differential pulse voltammetry (DPV) method. The detection limits for AA, DA, and UA in simultaneous detection were calculated as 17.80 μM, 0.018 μM, and 0.068 μM (S/N = 3), respectively. Furthermore, the feasibility of using Co_2P hybrid-SPE for the simultaneous detection of AA, DA, and UA in real serum samples was also confirmed.

Received 5th March 2024
Accepted 23rd April 2024

DOI: 10.1039/d4ra01702a

rsc.li/rsc-advances

Introduction

Ascorbic acid (AA), dopamine (DA), and uric acid (UA) usually coexist in biological fluids, playing important roles in various physiological processes of the human body.[1] Abnormal levels of these small molecules are usually correlated with diseases, such as scurvy, Parkinson's disease, and gout.[2–4] Therefore, they are usually employed as biomarkers for the clinical screening of diseases. The simultaneous detection of these biomarkers not only provides insights into different aspects of health status but also offers a cost-effective and efficient strategy for the diagnosis of diseases. This is particularly attractive for point-of-care testing (POCT) applications and source-limited regions.

Among various detection strategies, the electrochemical detection method is an attractive tool to realize the simple and fast analysis of multiple analytes with low cost.[5] However, due to the similar oxidation potentials of AA, DA and UA, it is hard for a traditional electrode to clearly separate the signals for these three analytes from a mixture, making it difficult to precisely detect individual biomarkers.[6] Transition-metal-based nanomaterials have been considered promising catalysts for improving electrochemical sensing performance, leveraging their various valence states and large surface area.[7,8] For example, Lu and coworkers[9] synthesized cobalt oxide nanoparticles decorated on an N-doped carbon-based substrate for the simultaneous detection of DA and UA using the redox pair of Co(II)/Co(III). Polydopamine was utilized as a nitrogen source as well as a connecting agent between the carbon substrate and cobalt oxide particles, which can facilitate electron transfer to alleviate the low conductivity issue associated with cobalt oxides. Additional efforts are still desired for the further development of a catalyst with superior electrochemical sensing performance for the simultaneous detection of AA, DA, and UA.

Transition metal phosphides with nearly metallic properties have shown outstanding electrical conductivity in electrochemical sensing.[10,11] Moreover, by coupling them with an N-doped porous carbon matrix, the different electronegativities of P, C, and N elements offer various possibilities to tailor the electronic structure of the material, thereby tuning the electrocatalytic performance.[12,13] Metal–organic frameworks (MOFs) with tunable compositions have recently proved an excellent template to synthesize heteroatom-doped porous carbon-based materials for electrochemical catalysis.[14,15] The heteroatom-embedded porous carbon substrate not only provides enhanced electrical conductivity but also preserves the dispersion of active sites for electrocatalytic reactions, both of which are of great significance for electrochemical sensing.[16–19]

In this study, we report a facile method to synthesize a cobalt phosphide (Co_2P) hybrid for the simultaneous electrochemical detection of AA, DA, and UA through pyrolysis of the MOF precursor and *in situ* phosphating. The nearly metallic properties of transition metal phosphides and the heteroatom-doped

Key Laboratory of Biorheological Science and Technology, Ministry of Education and Bioengineering College, Chongqing University, Chongqing, 400044, China. E-mail: biojdeng@cqu.edu.cn

† Electronic supplementary information (ESI) available. See DOI: https://doi.org/10.1039/d4ra01702a

porous carbon substrate in the as-synthesized hybrid contribute to the improved electrocatalytic performance of the hybrid. By preparing a Co_2P hybrid-modified screen-printed electrode (Co_2P hybrid-SPE), simultaneous detection of AA, DA, and UA was performed with high sensitivity and specificity using the differential pulse voltammetry (DPV) method. Furthermore, the feasibility of Co_2P hybrid-SPE for the simultaneous detection of the three analytes in real serum samples was confirmed.

Experimental

Materials

Phosphate buffer saline (PBS, 0.1 M, pH 7.0) was purchased from Source Leaf Biotechnology (Shanghai, China). Potassium ferricyanide ($K_3Fe(CN)_6$, ≥99.5%), isopropyl alcohol (≥99.7%) and potassium chloride (KCl, 99.5%) were provided by Aladdin (Shanghai, China). Dopamine hydrochloride (DA) and uric acid (UA, ≥99%) were obtained from Sigma-Aldrich (St. Louis, MO, USA). L-Ascorbic acid (AA, >99%) citric acid (CA, 99.5%), L-cysteine (L-Cys, 99%), sodium carbonate (Na_2CO_3, 99.5%), calcium chloride ($CaCl_2$, 99.99%), and magnesium sulfate ($MgSO_4$, 99.5%) were bought from Macklin (Shanghai, China). Ethanol, zinc nitrate hexahydrate ($Zn(NO_3)_2\cdot 6H_2O$, 99%), cobalt nitrate hydrate ($Co(NO_3)_2\cdot 6H_2O$, 99%), dibasic sodium phosphate (Na_2HPO_4) and 2-methylimidazole ($C_4H_6N_2$, 98%) were obtained from Adamas (Shanghai, China). All of the chemicals were used without further purification. The water used in the experiments was obtained from a Milli-Q system (18.2 MΩ cm^{-1}).

Synthesis of Co_2P hybrid

A nitrate salt aqueous solution was first prepared by dissolving 0.59 g of $Zn(NO_3)_2\cdot 6H_2O$ and 0.57 g of $Co(NO_3)_2\cdot 6H_2O$ in 8 mL of deionized water, followed by mixing with 80 mL of deionized water containing 22.7 g of 2-methylimidazole under magnetic stirring for 5 hours at room temperature, forming ZnCo-MOF. The as-prepared ZnCo-MOF was washed with deionized water through centrifugation at 10 k rpm three times, followed by freeze-drying for 12 hours to obtain ZnCo-MOF powder. To synthesize the cobalt phosphide hybrid, the ZnCo-MOF powder was put into a tube furnace (SLG-1100-60, Shengli Testing Instruments, Shanghai, China) for pyrolysis under a nitrogen atmosphere. Na_2HPO_4 was placed upstream as the phosphorus source. Thermal treatments of 300 °C for 2 hours and 900 °C for 2 hours were applied to the ZnCo-MOF and the final Co_2P hybrid was achieved after natural cooling at room temperature.

Preparation of Co_2P hybrid-modified SPE

A three-electrode system-based SPE (Weihai Poten Technology, Shandong, China) was employed for the electrochemical measurements. The working and counter electrodes were carbon-based electrodes and the reference electrode was an Ag/AgCl electrode. The diameter of the working electrode was 4 mm. The Co_2P hybrid ink was prepared by dissolving 2 mg of Co_2P hybrid powder into 1 mL of isopropyl alcohol solution. The Co_2P hybrid-SPE was fabricated by dropping 15 μL of Co_2P hybrid ink onto the working electrode of the SPE and naturally dried at room temperature.

Electrochemical measurements

To perform the electrochemical measurement, 100 μL of sample solution was dropped onto the surface of Co_2P hybrid-SPE using a micropipette. The cyclic voltammetry (CV) and differential pulse voltammetry (DPV) measurements were performed with a CHI660E workstation (Shanghai, China). The CV measurements were conducted at a scan rate of 50 mV s^{-1} in the potential range of −0.3 to 0.7 V. The DPV measurements were performed with an amplitude of 50 mV and a pulse period of 0.5 s in the potential range of −0.3 to 0.7 V.

Characterization

The morphologies and microstructures of the as-synthesized Co_2P hybrid were characterized with a field-emission scanning electron microscope (FE-SEM, Zeiss Gemini SEM360, 2 kV) and a transmission electron microscope (TEM, Talos F200X, 200 kV, Thermo Scientific, USA) equipped with an energy dispersive spectrometer (EDS). X-ray diffraction (XRD, Bruker D8 advance) with Cu Kα radiation (λ = 1.54 Å) was employed to investigate the crystallographic information for the obtained Co_2P hybrid. The valence states of the Co_2P hybrid were analyzed with an X-ray photoelectron spectroscope (XPS, ESCALAB 250 Xi) with Al Kα radiation.

Results and discussion

Synthesis and characterization of Co_2P hybrid

The synthesis of the hybrid is illustrated in Scheme 1. The hybrid was obtained by pyrolysis of the ZnCo-MOF precursor under nitrogen gas in a tube furnace with Na_2HPO_4 serving as the phosphorous source. During the thermal treatment process, dispersed cobalt phosphide nanoparticles were formed on a P,

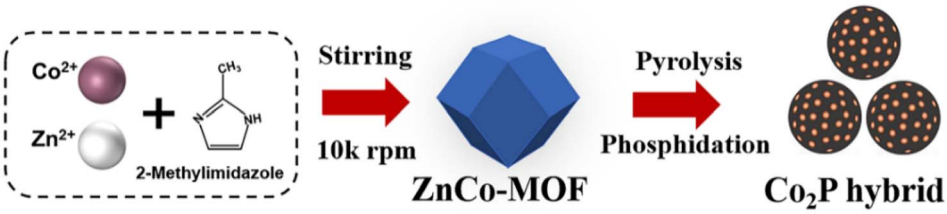

Scheme 1 Schematic illustration of the synthesis of cobalt phosphide hybrid.

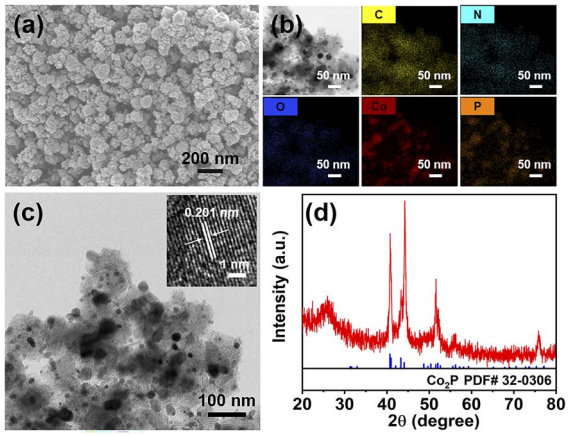

Fig. 1 SEM image (a), elemental mapping images (b), TEM image (c), and XRD pattern (d) of the cobalt phosphide hybrid. Inset in (c) is the HRTEM image of a cobalt phosphide nanoparticle.

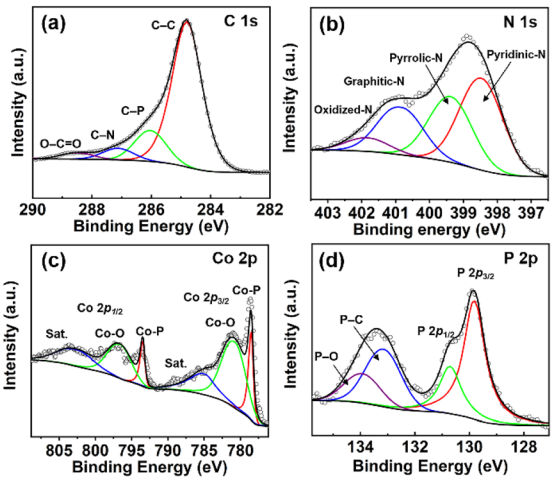

Fig. 2 High-resolution XPS spectra of (a) C 1s, (b) N 1s, (c) Co 2p, and (d) P 2p for the Co_2P hybrid.

N-doped porous carbon substrate after the evaporation of Zn species and carbonization of the nitrogen-rich organic linkers.

The SEM image of the obtained cobalt phosphide hybrid is shown in Fig. 1a. Nanoparticles with a rough morphology are distributed on the substrate and form a porous structure, which is beneficial for exposing abundant active sites. The elemental mapping results demonstrate the presence of C, N, O, Co and P elements in the hybrid (Fig. 1b). Moreover, the overlapping distribution of Co and P elements suggests the formation of cobalt phosphide compound. The TEM image confirms the formation of dispersed nanoparticles on the substrate (Fig. 1c). The high-resolution TEM (HRTEM) image of the nanoparticle indicates a lattice fringe of 0.201 nm, corresponding to the (211) plane of Co_2P (inset in Fig. 1c).[20] Fig. 1d displays the XRD pattern of the hybrid. The diffraction peaks at around 40.8°, 43.4°, 44.3° and 51.6° belong to the (121), (211), (130), and (131) planes of Co_2P (JCPDS 32-0306), respectively.[21] This further demonstrates the formation of Co_2P in the hybrid.

The chemical valence information for the Co_2P hybrid was investigated by the XPS method. The full survey spectrum demonstrates the co-existence of Co, O, N, C and P elements in the hybrid (Fig. S1†). As shown in Fig. 2a, the high-resolution C 1s spectrum can be divided into four peaks with binding energies of 284.8 eV, 286.0 eV, 287.1 eV and 288.4 eV, which are assigned to C–C, C–P, C–N and O–C=O, respectively.[22] The high-resolution N 1s spectrum can be deconvoluted into four peaks, which are ascribed to pyridinic-N (398.5 eV), pyrrolic-N (399.4 eV), graphitic-N (400.8 eV), and oxidized-N (401.8 eV), respectively (Fig. 2b).[23,24] The presence of pyridinic-N, pyrrolic-N, and graphitic-N can contribute to abundant electroactive sites and high conductivity by modulating the electronic structure of the carbon matrix with their lone pair of electrons.[18] The formation of oxidized-N is due to the exposure of the hybrid surface to the air. In the high-resolution Co 2p spectrum, the peaks at 778.4 eV and 793.4 eV are the Co $2p_{3/2}$ and Co $2p_{1/2}$ peaks of Co–P, respectively (Fig. 2c).[24] The peaks at 785.7 eV and 803.2 eV are satellite peaks. The presence of peaks at 781.0 eV and 796.8 eV results from the surface oxidation of Co species in the hybrid.[25] As shown in Fig. 2d, the peaks at 129.8 eV and 130.7 eV in the P 2p spectrum can be indexed to the P $2p_{3/2}$ and P $2p_{1/2}$ peaks of Co_2P, respectively.[20] The peaks at 133.1 eV and 133.9 eV in the P 2p spectrum indicate the formation of P–C, and P–O, respectively.[26,27]

Electrochemical behavior of Co_2P hybrid-SPE

The electrocatalytic performance of the Co_2P hybrid was evaluated by modifying the hybrid on an SPE to form Co_2P hybrid-SPE. The electrochemical behavior of the as-prepared Co_2P hybrid-SPE was first explored in 0.1 M KCl aqueous solution containing 5 mM $K_3Fe(CN)_6$ using CV measurement. A bare SPE was adopted for comparison. As shown in Fig. 3a, Co_2P hybrid-SPE displays an obvious enhancement in current response compared with the bare SPE, indicating an enhanced electron transfer between the analyte and the electrode. In addition,

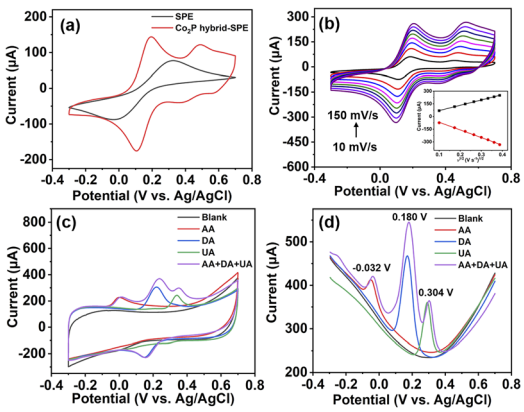

Fig. 3 CV response for 5 mM $K_3Fe(CN)_6$ in 0.1 M KCl aqueous solution on Co_2P hybrid-SPE (a) at a scan rate of 50 mV s^{-1} with bare SPE as a comparison, and (b) at various scan rates. CV curves (c) and DPV curves (d) of Co_2P hybrid-SPE in 0.1 M PBS aqueous solution for the individual and simultaneous detection of 3 mM AA, 100 μM DA, and 100 μM UA.

pairs of redox peaks are observed in the CV curve of Co_2P hybrid-SPE, corresponding to $[Fe(CN)_6]^{3-/4-}$, and redox peaks of Co_2P, respectively.[28] However, only one pair of $[Fe(CN)_6]^{3-/4-}$ peaks can be observed in the CV curve of bare SPE. Fig. 3b shows the CV responses of Co_2P hybrid-SPE at different scan rates for 5 mM $K_3Fe(CN)_6$ in 0.1 M KCl aqueous solution. The current response increases with the scan rate in the range from 10 mV s^{-1} to 150 mV s^{-1}. A linear relationship between the peak current and the square root of scan rate can be achieved (inset in Fig. 3b), indicating a diffusion-controlled process on the Co_2P hybrid-SPE.[29] The electroactive surface area of Co_2P hybrid-SPE was calculated with the Randles–Ševčík equation,[28]

$$I_p = 2.69 \times 10^5 \times n^{3/2} A D^{1/2} \nu C \quad (1)$$

where I_p is the oxidation peak current (A); n indicates the number of electrons transferred in $[Fe(CN)_6]^{3-/4-}$ ($n = 1$); A indicates the electroactive surface area (cm^2); D is the diffusion coefficient of $[Fe(CN)_6]^{3-/4-}$ (6.70×10^{-6} cm^2 s^{-1}); ν is the scan rate; and C is the concentration of the redox analyte. The calculated electroactive surface area of Co_2P hybrid-SPE is 0.18 cm^2, while the electroactive surface area of bare SPE is 0.09 cm^2 (Fig. S2†). The larger electroactive surface area of Co_2P hybrid-SPE is beneficial for facilitating electron transfer and providing abundant active sites.[30]

The feasibility of Co_2P hybrid-SPE for the detection of AA, DA, and UA in 0.1 M PBS was then evaluated using CV and DPV methods. As shown in Fig. 3c, compared with the response in 0.1 M PBS, the CV curve of Co_2P hybrid-SPE shows a noticeable increase in the oxidation current at around 0.001 V, 0.220 V and 0.340 V, respectively, after individual additions of 3 mM AA, 100 μM DA and 100 μM UA in 0.1 M PBS solutions, attributed to the oxidation of AA, DA, and UA, respectively. After the simultaneous addition of 3 mM AA, 100 μM DA, and 100 μM UA, the CV response of Co_2P hybrid-SPE exhibits three well-separated peaks, showing similar oxidation potentials to those identified in the CV curves achieved by the individual detection of these species. Similar well-resolved peaks were observed in the DPV curve after the separate and simultaneous addition of 3 mM AA, 100 μM DA, and 100 μM UA (Fig. 3d). The potentials of the oxidation peaks for AA, DA, and UA in the simultaneous detection DPV curve are at around −0.032 V, 0.180 V, and 0.304 V, respectively. The peak-to-peak potential differences are 212 mV, 124 mV, and 336 mV for DA–AA, UA–DA, and UA–AA, respectively. The well-defined oxidation peaks indicate the capability of Co_2P hybrid-SPE for the simultaneous detection of these three analytes.

Detection of DA, UA, and AA using Co_2P hybrid-SPE

The DPV method was used to perform the individual and simultaneous determination of AA, DA, and UA using Co_2P hybrid-SPE. The individual detection of AA, DA, and UA was first performed in the presence of the other two analytes. During the analysis, the concentration of the target analyst was varied, while the concentrations of the other two analytes were kept constant. Fig. 4a shows the DPV response of Co_2P hybrid-SPE for different concentrations of AA in 0.1 M PBS, while the concentrations of DA and UA were maintained at 5 μM and 30 μM, respectively. The oxidation peak current increases as the AA concentration rises from 0.1 mM to 5.5 mM, while the peak currents for DA and UA remain relatively unchanged. This indicates that the variation in concentration of AA does not interfere with the peak currents of DA and UA. The current response of Co_2P hybrid-SPE for AA was further plotted as a function of AA concentration, which indicates a linear detection range from 0.1 mM to 4.5 mM with a sensitivity of 0.18 μA μM^{-1} cm^{-2} (Fig. 4b). The detection limit was calculated as 12.15 μM (S/N = 3).

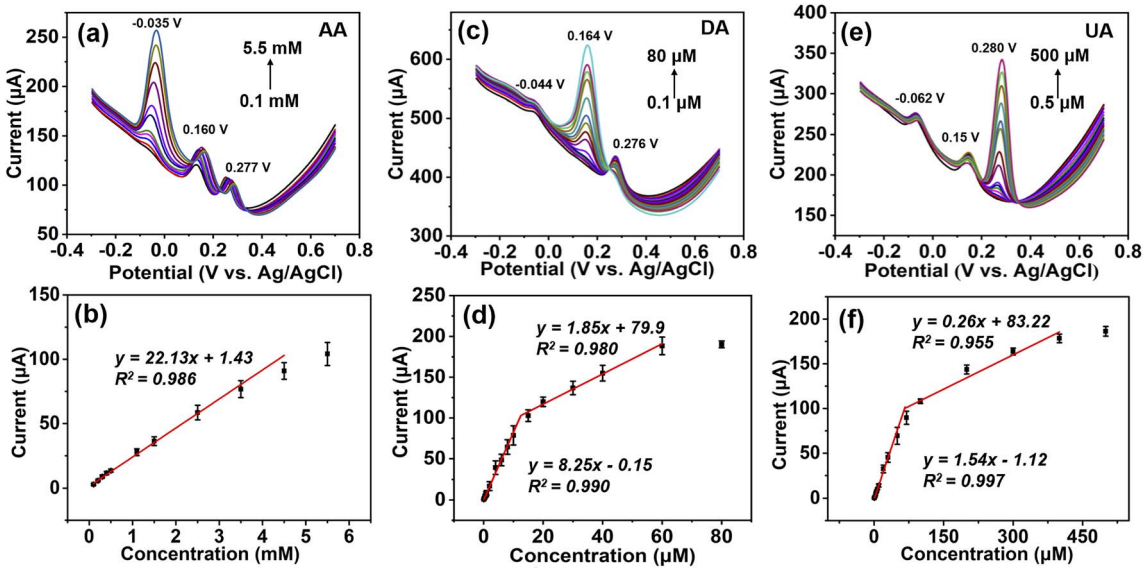

Fig. 4 DPV responses (a, c, e) and the corresponding calibration curves (b, d, f) of Co_2P hybrid-SPE in 0.1 M PBS containing (a and b) 5 μM DA and 30 μM DA for different concentrations of AA, (c and d) 1 mM AA, and 30 μM UA for different concentrations of DA, and (e and f) 1 mM AA and 5 μM DA for different concentrations of UA.

A similar trend can be observed for the individual detection of DA and UA in the presence of the other two analytes with constant concentrations, respectively (Fig. 4c and e). The current response of Co_2P hybrid-SPE for DA exhibits two linear detection ranges in the presence of 1 mM AA and 30 μM UA: 0.1 μM to 10 μM with a sensitivity of 65.68 μA μM^{-1} cm^{-2}, and 10 μM to 60 μM with a sensitivity of 14.73 μA μM^{-1} cm^{-2}, respectively (Fig. 4d). The detection limit was calculated as 0.015 μM (S/N = 3). Co_2P hybrid-SPE shows two linear detection ranges for UA in the presence of 1 mM AA and 5 μM DA: 0.5 μM to 70 μM with a sensitivity of 12.26 μA μM^{-1} cm^{-2}, and 70 μM to 400 μM with a sensitivity of 2.07 μA μM^{-1} cm^{-2}, respectively (Fig. 4f). The detection limit was calculated as 0.092 μM (S/N = 3). Due to the stronger adsorption of DA and UA on the hybrid substrate, a lower detection limit for DA and UA can be achieved than that for AA using the Co_2P hybrid.[31,32] Moreover, the stronger adsorption enables multilayer adsorption of DA and UA molecules on the electrode surface with different interaction strengths with the substrate, resulting in two linear detection ranges.[33,34]

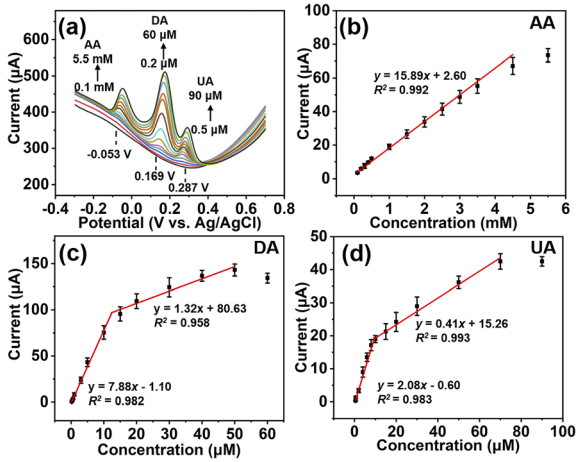

Fig. 5 DPV responses of Co_2P hybrid-SPE (a) and the corresponding calibration curves of the peak current *versus* the concentration of AA (b), DA (c), and UA (d) by varying their concentrations simultaneously.

Simultaneous detection of AA, DA, and UA was carried out by varying the concentrations of these three analytes at the same time. As shown in Fig. 5a, the oxidation peak currents for AA, DA, and UA increase simultaneously with the concentrations of these three analytes. The oxidation peaks remain well separated during the simultaneous variation of their concentrations. The Co_2P hybrid-SPE shows a linear detection range from 0.1 mM to 4.5 mM for AA with a sensitivity of 0.13 μA μM^{-1} cm^{-2} (Fig. 5b). Two linear detection ranges (0.2 μM to 10 μM, and 10 μM to 50 μM) can be achieved for DA detection with sensitivities of 62.74 μA μM^{-1} cm^{-2} and 10.51 μA μM^{-1} cm^{-2}, respectively (Fig. 5c). The Co_2P hybrid-SPE exhibits two linear detection ranges for UA: 0.5 μM to 10 μM with a sensitivity of 16.56 μA μM^{-1} cm^{-2}, and 10 μM to 70 μM with a sensitivity of 3.26 μA μM^{-1} cm^{-2}, respectively. The sensitives for AA, DA, and UA are close to those in individual detection results, which further indicates these three analytes do not significantly interfere with each other during simultaneous detection. The detection limits for AA, DA, and UA were calculated as 17.80 μM, 0.018 μM and 0.068 μM (S/N = 3), respectively. Table 1 summarizes the sensing performance of recently reported electrochemical sensors in the literature. It is found that the proposed Co_2P hybrid-SPE demonstrates superior sensing performance compared with most reported electrochemical sensors in the simultaneous detection of AA, DA, and UA.

Anti-interference, reproducibility and stability analyses

The anti-interference ability of Co_2P hybrid-SPE was evaluated by measuring the current response in a 0.1 M PBS solution containing 2 mM AA, 5 μM DA, and 30 μM UA in the presence of interference species of 1 mM citric acid (CA), 1 mM glucose (Glu), 1 mM L-cysteine (L-Cys), 1 mM Na_2CO_3, 1 mM KCl, 1 mM $MgSO_4$, and 1 mM $CaCl_2$. As shown in Fig. 6a, compared with the current response for a blank sample (without interference species), Co_2P hybrid-SPE shows a negligible change (<4.5%) in the current response for 2 mM AA, 5 μM DA, and 30 μM UA in the presence of interference.

A reproducibility test of Co_2P hybrid-SPE was conducted by performing the DPV measurement under the same conditions in

Table 1 Comparison of the proposed Co_2P hybrid-SPE with other electrochemical sensors for the simultaneous detection of AA, DA, and UA

	Linear range (μM)			Detection limit (μM)			
	AA	DA	UA	AA	DA	UA	Ref.
CoFe@G	500–8000	0.4–70	5–100	21.4	0.015	0.193	33
AuNPs@TS-COF/RGO	8–900	0.5–20, 20–100	0.5–25, 25–80	4.30	0.03	0.07	35
$MnFe_2O_4/MoS_2$	1000–6000	1–100	5–80	903	0.16	3.05	36
rGO/PPy-Pt	800–2100	30–1400	100–350	0.12	0.071	0.16	37
$ZnCo_2O_4$ NA/CC	10–500	0.5–100	0.5–100	7.79	0.31	0.37	38
Au–Pd/MXene/LSG	10–1600	12–240	8–100, 200–800	3	0.13	1.47	39
ZnO/PANI/CPE	100–1300	10–1400	10–120	63	29	7	40
Fe_3O_4 NP	1050–2300	10–100	20–160	95	4.5	14	41
3D-NG	20–10000	1–1000	0.5–600	3.91	0.26	0.12	42
GQDs/IL-SPCE	25–400	0.2–6	0.5–10	10.90	0.05	0.02	43
MNCS	10–2000	0.4–70	0.6–210	5.39	0.17	0.34	44
Co_2P hybrid	100–4500	0.2–10, 10–50	0.5–10, 10–70	17.80	0.018	0.068	This work

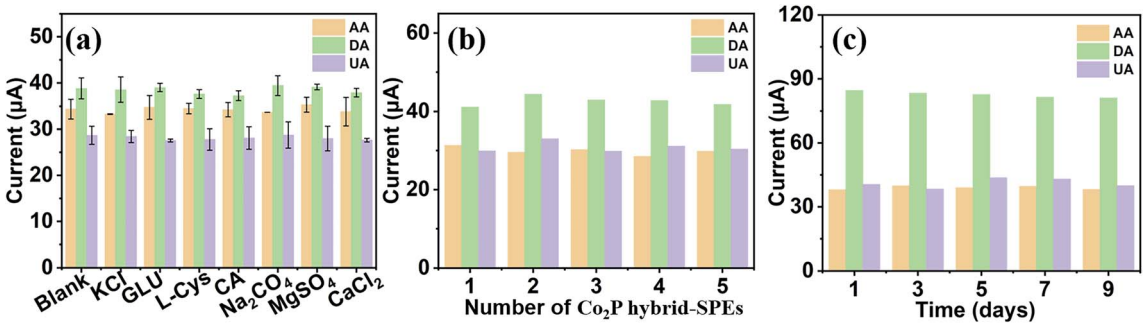

Fig. 6 The peak current of Co_2P hybrid-SPE in 0.1 M PBS aqueous solution containing (a) 2 mM AA, 5 μM DA, and 30 μM UA without and with interference species, (b) 1.5 mM AA, 5 μM DA, and 30 μM using 5 independent electrodes, and (c) 2.5 mM AA, 10 μM DA, and 30 μM UA on different days.

Table 2 Simultaneous determination of AA, DA, and UA in human serum samples using Co_2P hybrid-SPE

Sample	Species	Detected (μM)	Spiked (μM)	Found (μM)	RSD (%) ($n = 5$)	Recovery (%)
#1	AA	—	500	499.00 ± 20.88	4.18	99.80
	DA	—	5	5.19 ± 0.02	0.39	103.80
	UA	2.17	5	7.51 ± 0.578	7.70	104.71
#2	AA	—	1000	1032.00 ± 23.49	2.28	103.20
	DA	—	10	10.22 ± 0.40	3.92	102.20
	UA	1.84	10	11.91 ± 0.92	7.70	100.61
#3	AA	—	3000	2940.00 ± 160.00	5.44	98.00
	DA	—	30	29.92 ± 0.51	1.70	99.70
	UA	1.93	30	32.09 ± 1.19	3.70	100.5

a mixture of 1.5 mM AA, 5 μM DA, and 30 μM UA using 5 independent Co_2P hybrid-SPEs (Fig. 6b). Relative standard deviation (RSD) values of 3.41%, 2.94%, and 4.30% were achieved for AA, DA, and UA, respectively, indicating good reproducibility of Co_2P hybrid-SPE. The stability of Co_2P hybrid-SPE was assessed by measuring the current response of the prepared Co_2P hybrid-SPE for 2.5 mM AA, 10 μM DA, and 30 μM UA for 9 days. As shown in Fig. 6c, Co_2P hybrid-SPE retained 98.4%, 96.0%, and 98.5% of the initial responses for 2.5 mM AA, 10 μM DA, and 30 μM UA, respectively, after 9 days, suggesting good stability.

Determination of analytes in serum samples

To assess the practical application of Co_2P hybrid-SPE, the simultaneous determination of AA, DA, and UA was carried out in 100-fold diluted human serum samples using a spike-and-recovery method. The serum samples were collected from volunteers in Chongqing University Hospital and were used for the experiment with the consent of volunteers and Chongqing University Hospital. The serum samples were diluted with 0.1 M PBS and spiked with different concentrations of AA, DA, and UA, simultaneously. The DPV method was used for measurement. As shown in Table 2, the Co_2P hybrid-SPE shows good recovery and RSD (<8.0%) for the simultaneous detection of the three analytes.

Conclusions

In summary, a Co_2P hybrid has been synthesized through a facile MOF-derived method and it demonstrated its superior ability in the simultaneous detection of AA, DA, and UA using the synergistic effect between the Co_2P nanoparticles and the P, N-doped porous carbon substrate. The as-prepared Co_2P hybrid-SPE exhibited well-resolved oxidation peaks and enhanced current response for the simultaneous detection of AA, DA, and UA with high sensitivity and specificity. Detection limits for AA, DA, and UA in the simultaneous detection were calculated as 17.80 μM, 0.018 μM, and 0.068 μM (S/N = 3), respectively. Furthermore, the Co_2P hybrid-SPE demonstrated its effectiveness in the simultaneous determination of AA, DA, and UA in human serum samples, indicating its potential in clinical diagnostic applications.

Conflicts of interest

There are no conflicts to declare.

Acknowledgements

This work was supported by the National Natural Science Foundation of China (No. 32101114), China Postdoctoral Science Foundation (No. 2021M700603).

References

1 M. Sajid, M. K. Nazal, M. Mansha, A. Alsharaa, S. M. S. Jillani and C. Basheer, *TrAC, Trends Anal. Chem.*, 2016, **76**, 15–29.
2 A. Arroquia, I. Acosta and M. P. G. Armada, *Mater. Sci. Eng., C*, 2020, **109**, 110602.

3 C. Mehler-Wex, P. Riederer and M. J. N. R. Gerlach, Neurotoxic, *Research*, 2006, **10**, 167–179.
4 Y. Xing, C. Lv, Y. Fu, L. Luo, J. Liu, X. Xie and F. Chen, *Talanta*, 2024, **271**, 125674.
5 S. Li, H. Zhang, M. Zhu, Z. Kuang, X. Li, F. Xu, S. Miao, Z. Zhang, X. Lou, H. Li and F. Xia, *Chem. Rev.*, 2023, **123**, 7953–8039.
6 G. S. Geleta, *Sens. Bio-Sens. Res.*, 2024, **43**, 100610.
7 A. S. Agnihotri, A. Varghese and N. M, *Appl. Surf. Sci. Adv.*, 2021, **4**, 100072.
8 Y. H. Wang, K. J. Huang and X. Wu, *Biosens. Bioelectron.*, 2017, **97**, 305–316.
9 N. Lu, Y. Liu, X. Yan, Z. Xu, Y. Xing, Y. Song, P. Zhao, M. Liu, Y. Gu, Z. Zhang and S. Zhai, *ACS Appl. Nano Mater.*, 2022, **5**, 11361–11370.
10 S. Lakshmy, S. Santhosh, N. Kalarikkal, C. S. Rout and B. Chakraborthy, *J. Appl. Phys.*, 2023, **133**, 070702.
11 D. Yin, J. Tang, R. Bai, S. Yin, M. Jiang, Z. Kan, H. Li, F. Wang and C. Li, *Nanoscale Res. Lett.*, 2021, **16**, 11.
12 Z. Y. Wang, Z. Y. Tsai, H. W. Chang and Y. C. Tsai, *Micromachines*, 2024, **15**, 105.
13 Y. Wang, M. Wu, J. Li, H. Huang and J. Qiao, *J. Mater. Chem. A*, 2020, **8**, 19043–19049.
14 M. Adeel, K. Asif, M. M. Rahman, S. Daniele, V. Canzonieri and F. Rizzolio, *Adv. Funct. Mater.*, 2021, **31**, 2106023.
15 X. Tang, N. Li and H. Pang, *Green Energy Environ.*, 2022, **7**, 636–661.
16 Y. Xie, C. Feng, Y. Guo, S. Li, C. Guo, Y. Zhang and J. Wang, *Appl. Surf. Sci.*, 2021, **536**, 147786.
17 Y. Shen, T. Pan, L. Wang, Z. Ren, W. Zhang and F. Huo, *Adv. Mater.*, 2021, **33**, 2007442.
18 M. Y. Emran, M. A. Shenashen, A. Elmarakbi, M. M. Selim and S. A. El-Safty, *Anal. Chim. Acta*, 2022, **1192**, 339380.
19 H. Wang, T. Maiyalagan and X. Wang, *ACS Catal.*, 2012, **2**, 781–794.
20 W. Xu, G. Fan, S. Zhu, Y. Liang, Z. Cui, Z. Li, H. Jiang, S. Wu and F. Cheng, *Adv. Funct. Mater.*, 2021, **31**, 2107333.
21 D. Das and K. K. Nanda, *Nano Energy*, 2016, **30**, 303–311.
22 B. Wang, Y. Chen, Q. Wu, Y. Lu, X. Zhang, X. Wang, B. Yu, D. Yang and W. Zhang, *J. Mater. Sci. Technol.*, 2021, **74**, 11–20.
23 Y. Wen, J. Qi, P. Wei, X. Kang and X. Li, *J. Mater. Chem. A*, 2021, **9**, 10260–10269.
24 D. Zhang, P. Sun, Z. Zuo, T. Gong, N. Huang, X. Lv, Y. Sun and X. Sun, *J. Electroanal. Chem.*, 2020, **871**, 114327.
25 C. Fu, S. Lin, C. Zhao, J. Wang, L. Wang, J. L. Bao, Y. Wang and T. Liu, *Energy Storage Mater.*, 2022, **45**, 1109–1119.
26 M. Yang, F. Feng, K. Wang, S. Li, X. Huang, L. Gong, L. Ma and R. Li, *ChemSusChem*, 2020, **13**, 351–359.
27 J. Wu, X. Yang, J. Zhang, S. Guan, J. Han, J. Wang, K. Li, G. Zhang and T. Guan, *J. Power Sources*, 2022, **548**, 232065.
28 L. Xiao, S. Zheng, K. Yang, J. Duan and J. Jiang, *Microchem. J.*, 2021, **168**, 106432.
29 Q. Azizpour Moallem and H. Beitollahi, *Microchem. J.*, 2022, **177**, 107261.
30 Y. Xia, G. Li, Y. Zhu, Q. He and C. Hu, *Microchem. J.*, 2023, **190**, 108726.
31 A. Cecilia Rossi Fernández, L. Alejandra Meier and N. Jorge Castellani, *Comput. Theor. Chem.*, 2022, **1212**, 113705.
32 K. Prasert and T. Sutthibutpong, *Sensors*, 2021, **21**, 2773.
33 C. Hang, Y. Qin, G. Tian, J. Hu, W. Li and J. Wu, *Adv. Mater. Interfaces*, 2022, **9**, 2200774.
34 H. Y. Yue, S. Huang, J. Chang, C. Heo, F. Yao, S. Adhikari, F. Gunes, L. C. Liu, T. H. Lee, E. S. Oh, B. Li, J. J. Zhang, T. Q. Huy, N. V. Luan and Y. H. Lee, *ACS Nano*, 2014, **8**, 1639–1646.
35 M. Wang, H. Guo, N. Wu, J. Zhang, T. Zhang, B. Liu, Z. Pan, L. Peng and W. Yang, *Colloids Surf., A*, 2022, **634**, 127928.
36 P. Wu, Y. Huang, X. Zhao, D. Lin, L. Xie, Z. Li, Z. Zhu, H. Zhao and M. Lan, *Microchem. J.*, 2022, **181**, 107780.
37 R. Darabi, H. Karimi-Maleh, M. Akin, K. Arikan, Z. Zhang, R. Bayat, M. Bekmezci and F. Sen, *Electrochim. Acta*, 2023, **457**, 142402.
38 Z. Hu, P. Zhao, J. Li, Y. Chen, H. Yang, J. Zhao, J. Dong, N. Qi, M. Yang, D. Huo and C. Hou, *Anal. Methods*, 2022, **14**, 4330–4337.
39 Y. Wang, P. Zhao, B. Gao, M. Yuan, J. Yu, Z. Wang and X. Chen, *Microchem. J.*, 2023, **185**, 108177.
40 Y. Kadri, I. Bekri-Abbess and P. Herrasti, *Electroanalysis*, 2022, **35**, 2200248.
41 E. Gaya, N. Menendez, E. Mazario and P. Herrasti, *Chemosensors*, 2023, **11**, 79.
42 J. Jiang, D. Ding, J. Wang, X. Lin and G. Diao, *Analyst*, 2021, **146**, 964–970.
43 K. Kunpatee, S. Traipop, O. Chailapakul and S. Chuanuwatanakul, *Sens. Actuators, B*, 2020, **314**, 128059.
44 Y. Wang, Q. Dai, L. Yang, Y. Liu, C. Yu, C. Yao and X. Xu, *J. Electroanal. Chem.*, 2020, **873**, 114462.